Molecular interaction and inhibition of SARS-CoV-2 binding to the ACE2 receptor

Jinsung Yang
Louvain Institute of Biomolecular Science and Technology, Université catholique de Louvain, Louvain-la-Neuve, Belgium
Simon Petitjean
Louvain Institute of Biomolecular Science and Technology, Université catholique de Louvain, Louvain-la-Neuve, Belgium
Sylvie Derclaye
Louvain Institute of Biomolecular Science and Technology, Université catholique de Louvain, Louvain-la-Neuve, Belgium
Melanie Koehler
Louvain Institute of Biomolecular Science and Technology, Université catholique de Louvain, Louvain-la-Neuve, Belgium
Qingrong Zhang
Louvain Institute of Biomolecular Science and Technology, Université catholique de Louvain, Louvain-la-Neuve, Belgium
Andra C. Dumitru
Louvain Institute of Biomolecular Science and Technology, Université catholique de Louvain, Louvain-la-Neuve, Belgium
Patrice Soumillion
Louvain Institute of Biomolecular Science and Technology, Université catholique de Louvain, Louvain-la-Neuve, Belgium
David Alsteens (david.alsteens@uclouvain.be)
Louvain Institute of Biomolecular Science and Technology, Université catholique de Louvain, Louvain-la-Neuve, Belgium

---

Research Article

Keywords: Atomic force microscopy, Coronavirus, SARS-CoV-2, ACE2, interaction, force spectroscopy, blocking, inhibition, AFM, single-molecule

Posted Date: May 21st, 2020

DOI: https://doi.org/10.21203/rs.3.rs-30468/v1

Version of Record: A version of this preprint was published at Nature Communications on September 11th, 2020. See the published version at https://doi.org/10.1038/s41467-020-18319-6.

Abstract

Study of virus entry into cells is of critical importance for a better understanding of the interactions established between the viral glycoproteins and their receptors at the cell surface and could help to develop novel antiviral strategies. The novel coronavirus (SARS-CoV-2) entry into host cells is mediated by the transmembrane spike glycoprotein (S-glycoprotein) and the angiotensin-converting enzyme 2 (ACE2) has been identified as a cellular receptor. Here, we used atomic force microscopy to investigate the molecular mechanisms by which the S- glycoprotein binds to the ACE2 receptor. We demonstrated, both on model surfaces and on living cells, that the receptor binding domain (RBD) serves as a binding interface within the S- glycoprotein with the ACE2 receptor and we extracted the kinetic and thermodynamic properties of this binding pocket. Altogether, these results give a dynamic picture of the established interaction in physiologically relevant conditions. Finally, we identified and tested several binding inhibitor peptides targeting the virus early attachment stages, offering new perspectives in the treatment of the SARS-CoV-2 infection.

Introduction

In December 2019, a novel coronavirus (CoV) was determined to be responsible for an outbreak of potentially fatal atypical pneumonia, ultimately defined as coronavirus disease- 19 (COVID-19), in Wuhan, China. This novel CoV, termed severe acute respiratory syndrome (SARS)-CoV-2, was found to share similarities with the SARS-CoV that was responsible for the SARS pandemic that occurred in 2002. The resulting outbreak of COVID-19 has emerged as a severe pandemic. The genome of SARS-CoV-2 shares about 80% identity with that of SARS- CoV and is about 96% identical to the bat coronavirus BatCoV RaTG13.1

CoV entry into host cells is mediated by the transmembrane spike (S) glycoprotein that forms homotrimers protruding from the viral surface (**Figure 1a**).2 The S-glycoprotein comprises two functional subunits responsible either for binding to the host cell receptor (S1-subunit including the receptor binding domain (RBD)) or for fusion of the viral and cellular membranes (S2 subunit). Recent studies claimed that angiotensin-converting enzyme 2 (ACE2), previously identified as the cellular receptor for SARS-CoV, is also the receptor of the new coronavirus (SARS-CoV-2) (**Figure 1b**).3 In the case of SARS-CoV, the S-glycoprotein on the virion surface mediates receptor recognition (**Figure 1c**) and membrane fusion.4,5 Recently, the high- resolution cryo-electron microscopy structure obtained on the full-length human ACE2 in the presence of the RBD of the S-glycoprotein of SARS-CoV-2 suggests simultaneous binding of two S-glycoprotein trimers to an ACE2 dimer6. The S2 subunit is further cleaved by host proteases located immediately upstream of the fusion peptide,7 leading to the activation of the glycoprotein that undergoes extensive irreversible conformational changes facilitating the membrane fusion process. Altogether, the information obtained so far highlight the fact that CoV entry into susceptible cells is a complex process that requires the concerted action of receptor-binding and proteolytic activation of the S-glycoprotein at the host cell surface to finally promote virus-cell membrane fusion. However so far direct evidence about the dynamics of the binding of S1-subunit to the ACE2 receptor at the single-molecule level is missing.

Here, we analyze the biophysical properties of the SARS-CoV-2 S-glycoprotein binding, on model surfaces and on living cells, to ACE2 receptors using force distance (FD) curve-based atomic force microscopy (FD-curve based AFM) (**Figure 1c**). We extract the kinetics and thermodynamics of the interactions established *in vitro* and compare the binding properties of both S1-subunit and RBD. Next, we test short ACE2-derived peptides targeting the viral S-glycoprotein as potent binding inhibitor peptides and observed a significant reduction in the binding properties.

Results

S1-subunit specifically binds to purified ACE2 receptors.

As SARS-CoV-2 binding to ACE2 receptors is thought to play a key role in the first binding steps at the cellular membrane,3 we used FD-curve based AFM to evaluate at the single-molecule level the binding strength of the interaction established between the glycosylated S1-subunit and ACE2 receptors on model surfaces (**Figure 2a**). To mimic cell-surface receptors *in vitro*, ACE2 receptors were covalently immobilized onto gold surfaces coated with OH- and COOH- terminated alkanethiols using carbodiimide conjugation (see Methods). These model surfaces were imaged by AFM and the thickness of the grafted layer was validated by a scratching experiment, revealing a deposited layer of ~ 2.3 ± 1.0 nm (see Methods and **Supplementary Fig. 1**). To study the interaction between the S1-subunit and the immobilized ACE2 receptors, we covalently grafted the purified S1-subunit or RBD to the free end of a long polyethylene glycol (PEG)24 spacer attached to the AFM tip.8-10 Force-distance (FD) curves were recorded either with the S1-subunit or RBD functionalized tip over the ACE2 model surface to investigate the properties of the binding complex (**Figure 2b**). Specific adhesion events were observed on 5-10% of the retraction FD curves at rupture distances > 5 nm, which corresponds to the extension of the PEG linker (**Figure 2c**). To confirm the specificity of these interactions, we conducted additional independent control experiments using (*i*) an AFM tip only functionalized with the PEG linker or (*ii*) towards OH-/COOH-terminated alkanethiol surfaces missing the receptor. The binding frequency observed during those control experiments is significantly lower, thereby confirming the specificity of the S1-subunit/RBD – ACE2 complexes under our experimental conditions (**Figure 2c**).

Exploring the dynamics of S1-subunit – ACE2 interaction.

Single-molecule force-probing techniques, such as FD-based AFM measure the strength of a bond under an externally applied force, enabling to get insights into the binding free-energy landscape. According to the Bell-Evans model,11,12 an external force stressing a bond reduces the activation-energy barrier

toward dissociation and, hence, reduces the lifetime of the ligand-receptor pair (**Figure 2d**).13 The model predicts that far-from-equilibrium, the binding

strength of the ligand-receptor bond is proportional to the logarithm of the loading rate, LR, which describes the force applied on the bond over time. To investigate the kinetics of the probed complex, force distance curves were recorded at various retraction rates and contact times (**Figure 2e-h**). Dynamic force spectroscopy plots were obtained for both S1-subunit (**Figure 2e**) and RBD (**Figure 2f**) binding towards immobilized ACE2 receptors. In each case, the unbinding force increases linearly with the logarithm of the LR, as observed earlier for other virus-receptor bonds.9,14-17 The Bell-Evans model13 was used to fit the data enabling to interpret the binding-complex as a simple two-state model, in which the bound state is separated from the unbounded state by a single energy barrier (**Figure 2d**). From the slope of the fit, we estimated the length scale of the energy barrier (xu). We obtained very close values, xu = 0.81 ± 0.05 nm and 0.79 ± 0.04 nm for both the S1-subunit and RBD, showing that we are probing similar bonds (**Figure 2e,f**). The kinetic off-rate (koff) or dissociation rate is obtained from the intercept of the fit (at LR=0) yielding koff values of 0.008 ± 0.005 s-1 and 0.009 ± 0.006 s-1 for S1-subunit and RBD, respectively. These values are in good agreement with reported values obtained by surface plasmon resonance for the S-glycoprotein (koff = 0.003 s-1)18 and the RBD subunit (koff = 0.008 s-1) binding to ACE2 receptors19.

Assuming that the receptor-bond complex can be approximated by a pseudo first-order kinetics, we also estimated the kinetic on-rate (kon) from our single-molecule force spectroscopy experiments (**Figure 2g,h**).15 This association rate is extracted from the binding probability measured at various contact times and depends on the effective concentration described as the number of binding partners (ligand + receptor) within an effective volume Veff accessible under free-equilibrium interaction. Veff can be approximated by a half-sphere with a radius including the linker, the viral glycoprotein (S1-subunit or RBD) and the ACE2 receptor. For both the S1-subunit and RBD, we observed that the binding frequency increased exponentially with contact time and we extracted an interaction time of ~0.250 ms leading to a kon of 6.4 x 104 M-1 s-1 and 8.0 x 104 M-1 s-1, respectively. Finally, the dissociation constant KD is calculated as the ratio between the koff and the kon yielding values around ~120 nM for both complexes. This value corresponds to a high affinity interaction, confirming the specificity of the complexes established by SARS-Cov-2 with the ACE2 cell surface receptor, which in turn results in a long lifetime of the virus attachment to the cell surface, making the development of anti-binding molecules targeting this interaction more difficult. We also used optical

biolayer interferometry (BLI) to confirm the kinetic parameters characterizing this interaction and obtained very close affinities in the same nM range as AFM experiments (**Supplementary Fig. 2).** Our *in vitro* experiments confirm that SARS-CoV-2 binding to the ACE2 receptors is mediated by the RBD-ACE2 interface as our experimental conditions did not highlight any significant difference between S1-subunit and RBD binding.

Validation of the interaction on living cells.

Next, we wanted to investigate whether the interaction probed on isolated receptors is also established in physiologically relevant condition. To this end we performed binding assays on living A549 cells (human adenocarcinoma alveolar basal epithelial cells). While this cell line is widely used as a type II pulmonary epithelial cell model, it has been shown recently that those cells are incompatible with SARS-CoV-2 infection.20 Interestingly, ACE2 expression positively correlated with the differentiation state of epithelia. Although undifferentiated cells (cultured at low confluency) only express little ACE2, overexpression of ACE2 in undifferentiated A549 cells facilitated virus entry.21 We therefore co-cultured A549 cells (serving as control) with A549 cells transfected with ACE2-eGFP (A549-ACE2) (**Figure 3a**). Confocal images showed ACE2-eGFP receptors homogeneously distributing in small domains at the surface of A549 cells (**Figure 3b**). Guided by fluorescence (**Figure 3c**), we chose areas in which both cell types were in proximity to one another. Having both A549 cell types in one image area served as a direct control to evaluate whether interactions measured by the functionalized tip were indeed due to specific binding to fluorescent ACE2-eGFP receptors, and to evaluate the extent of unspecific interactions (**Figure 3c-e**). In such area, we simultaneously recorded a height image (**Figure 3d**) and corresponding adhesion map (**Figure 3e**), which were reconstructed from FD curves recorded for each topographic pixel. The retraction part of FD curves showed specific adhesion events mainly on A549-ACE2 cells, with a significantly higher binding probability (**Figure 3f**). Specific binding forces (and corresponding LR) were extracted from force *vs* time curves recorded on A549-ACE2 cells (**Figure 3g**) and overlaid on the DFS plot obtained on purified ACE2 receptors (**Figure 3h**). We observed a very good alignment between the data obtained on purified receptors and on living cells confirming the physiological relevance of our results obtained on model surfaces.

Inhibition of S1-subunit binding using ACE2-derived peptides.

Human recombinant soluble ACE2 (hrsACE2) is currently being considered for treatment of COVID-1922,23. However, ACE2 is involved in many key cellular processes such as blood pressure regulation and other cardiovascular functions. Therefore, hrsACE2 treatment could lead to dysregulation of those vital processes and subsequently cause deleterious effects for treated patients. To avoid any interference of the ACE2 homeostasis, we wanted to test whether small ACE2-derived peptides can also interfere with SARS-CoV-2 binding, by blocking binding sites on the S-glycoprotein. To this end, we synthetized four different peptides (sequences provided in **Supplementary Fig. 3**) which have been selected to mimic the regions of ACE2 that interact with the S1-subunit as determined by the crystal structure,24 and we tested

their binding inhibition properties using our single-molecule force spectroscopy approach (**Figure 4a,b**). We first measured the binding probability between the S1-subunit and the ACE2 in absence of peptide (0 µM), with a contact time of 250 ms, as reference and then injected our ACE-derived peptides at three different concentrations (1 µM, 10 µM and 100 µM. For the four peptides, we observed a progressive reduction of the binding probability as a function of the concentration confirming a specific inhibition. In addition, for each peptide, we noticed a reduction of >50% of the probed interactions already for the 1 µM concentration, suggesting a 50% inhibitory concentration (IC50) in the sub-µM range. The [22- 44] peptide shows the highest inhibition of the S1–ACE2 complex formation with a measured reduction in the binding probability of ~95%. The [22-57] peptide shows a similar inhibition potential (~90%), suggesting that the additional amino acids do not influence the overall affinity of the peptide for the S1-subunit. Overall, these results are in good agreement with the structural insights because these peptides are derived from the *N*-terminal helix of the ACE2 and therefore form with the RBD interface an important network of hydrophilic interactions (including 9 hydrogen bonds and a salt bridge). Within the ACE2-RBD complex, the [351-357] fragment is also part of a “hot binding spot” which results in our test by a good score with a reduction of ~70% of the initial specific binding probability. Finally, the [22-44-g- 351-357] peptide was also synthetized and tested based on the fact that in the crystal structure the distance between S44 and L351 is close enough to be filled by a single amino acid. A glycine residue was added between the two fragments because the two ACE2 fragments have opposite directionality and the glycine has a high propensity to form reverse

turns. Nevertheless, under our experimental conditions, we did not notice any improvement in the binding inhibition. Altogether, our *in vitro* assays at the single-molecule level provide direct evidence that ACE2-derived peptides are strong candidates to potentially inhibit SARS- CoV-2 binding to ACE2 receptors (**Figure 4c**).

ACE2-derived peptide inhibits specific binding on living cells.

Finally, we tested whether the [22-57] binding inhibition peptide could also prevent S1- subunit binding in the cellular context (**Figure 5**). The interaction between the S1-subunit and the confluent layer of a co-culture of A549 and A549-ACE2 cells was probed before and after addition of the peptide at 100 µM. Before injection, cells overexpressing the ACE2 receptors (A549-ACE2) shows higher binding probability (9.4 ± 1.6 % *vs* 19.4 ± 7.3 %, for A549 and A549- ACE2, respectively) (**Figure 5a-d**), in good agreement with our previous observation (**Figure 3f**). After injection of the [22-57] ACE2-derived peptide, we observed a significant decrease of the binding probability on both cell types (**Figure 5e,f**). In particular, the binding probability on A549-ACE2 cells significantly drops (~70%) reaching a level close to the one of the control

cells. Taking into account that undifferentiated A549 cells express little ACE2 and are poorly infected by CoV,21 this result supports the biological relevance of our ACE2-derived peptide acting as potential inhibitor capable of efficiently block SARS-CoV-2 binding.

Conclusions

In conclusion, we investigated the interaction established between the SARS-Cov-2 S- glycoprotein and the ACE2 receptor using single-molecule force spectroscopy. We demonstrated a specific binding mechanism between the S1-subunit and the ACE2 receptor. By comparing the binding of the S1-subunit and the RBD towards the ACE2 receptor, our experiment evidenced that both domains interact with the same kinetic and thermodynamic properties towards the ACE2 receptor highlighting that SARS-CoV-2 binding to ACE2 is dominated by the RBD/ACE2 interface. Our measurements show that under our physiologically relevant conditions, the RBD binds the ACE2 receptor with an intrinsic high- affinity (~120 nM) which could even be further stabilized at the whole virus level thanks to possible multivalent bonds between the S-glycoprotein trimer and ACE2 dimer.

Based on the available crystal structures of the molecular complex, we examined how several ACE2-derived peptide fragments could interfere with the S1-ACE2 complex formation. While all tested peptides show binding inhibition properties, peptides mimicking the N-terminal helix of the ACE2 receptor show the best results. Both [22-44] and [22-57] peptides exhibit an anti-binding activity with IC50 in the µM range resulting in a >90% decrease in the binding probability observed by AFM on purified receptor and >70% on living cells. On the cellular model, we observed that the binding probability drops to the level of the control cells (undifferentiated A549 cells) that are poorly infected by CoV.21 Therefore, those peptides appear as strong therapeutic candidates against the SARS-CoV-2 infection.

Methods

Cell culture and transfection. A549 cells (ATCC® CCL-185) were grown in Ham's F-12 Nutrient Mix with 10 % fetal bovine serum, penicillin (100 U ml−1), and streptomycin (100 µg mL−1) (Gibco) at 37 °C in a humidified atmosphere with 5% CO2. pcDNA3.1(+) ACE2-eGFP was transfected using Lipofectamine LTX (Invitrogen) according to the manufacturer’s protocol.

Functionalization of AFM tips. PFQNM-LC and MSCT-D cantilevers (Bruker) were used to probe the interaction between S1-subunit (Genscript, #U5377FC120) or RBD protein (Genscript, #U5377FC120) and ACE2 protein (Sino Biological, 90211-C02H). NHS-PEG24-Ph- aldehyde linkers were used to functionalize AFM tips as previously described.25 Briefly, the cantilevers were immersed in chloroform for 10 min and further cleaned in an UV radiation and ozone (UV-O) cleaner (Jetlight), and immersed overnight in an ethanolamine solution (3.3 g of ethanolamine in 6.6 ml of DMSO). They were washed with DMSO and ethanol 3 times, respectively. Ethanolamine-coated cantilevers were immersed in NHS-PEG24-Ph-

aldehyde solution (3.3 mg of it was diluted in 0.5 ml of chloroform and 30 µl of triethylamine) and finally washed 3 times with chloroform and dried with nitrogen.

For AFM tips functionalized with S1-subunit protein, 50 µl of S1-subunit protein solution (0.1 mg/ml) was put onto the cantilevers placed on Parafilm (Bemis NA) and 2 µl of fresh NaCNBH3 solution (6 % wt. vol-1 in 0.1 M NaOH(aq)) was mixed in the protein solution. The cantilevers were incubated in the solution for 1 hour on ice. Then, 5 µl of 1 M ethanolamine solution were carefully added to the protein solution and incubated 10 minutes to quench the reaction and finally washed three times with PBS.

For AFM tips derivatized with the RBD protein, 100 µl of a 100 µM tris-nitrilotriacetic amine 540 trifluoroacetate (Toronto Research Chemicals, Canada) (tris-NTA) solution was put onto the them placed on Parafilm and 2 ul of fresh NaCNBH3 solution was mixed in the protein solution. They were incubated in the solution for 1 hour on ice. Then, add 5 µl of 1 M ethanolamine solution in the protein solution and incubated 10 minutes. The mixture of 50 ul of RBD solution (0.1 mg/ml) and 2.5 µl 5 mM NiCl2 were put onto them and they were incubated for 2 hours. After incubation, they were washed in HEPES solution for 3 times.

Preparation of ACE2-coated model surfaces. ACE2 protein (Sino Biological, 90211-C02H) was immobilized using NHS-EDC chemistry. Gold-coated surfaces were first rinsed with ethanol, dried with a gentle stream of gas nitrogen, cleaned for 15 min by UV and ozone treatment (Jetlight) and incubated overnight in an alkanethiol solution (99 % 11-mercapto-1-undecanol

1 mM (Sigma Aldrich) and 1 % 16-mercaptohexadecanoic acid 1 mM (Sigma Aldrich) in ethanol). The chemically activated samples were rinsed with ethanol, dried with gas nitrogen and immersed for 30 min in the solution of 10 mg chemically activated -dimethylaminopropyl carbodiimide (Sigma Aldrich) and 40 mg of N-hydroxysuccinimide in 4 ml milliQ water. Finally, the surfaces were rinsed with milliQ water, incubated with ACE2 protein (0.1 µg/µL in PBS) on Parafilm (Bemis NA), washed in PBS.

FD-based AFM on model surfaces. FD-based AFM on model surfaces was performed in PBS at room temperature using functionalized MSCT-D probes (Bruker, nominal spring constant of

0.030 N/m and actual spring constants calculated using thermal tune).26 A Bioscope Resolve AFM (Bruker) operated in the force volume (contact) mode (Nanoscope software v9.1) was used. Areas of 5 x 5 µm were scanned, ramp size set to 500 nm and set point force of 500 pN, with a resolution of 32 x 32 pixels and a line frequency of 1 Hz.

Dynamic force spectroscopy (DFS) analysis (using a constant approach speed of 1 µm/s and variable retraction speeds of 0.1, 0.2, 1, 5, 10 and 20 µm/s) and kinetic on-rate estimation

measuring the binding probability for different hold times of 0, 50, 100, 150, 250, 500 and 1000 ms) were performed as described previously.9,27 The curves were analysed using Nanoscope analysis (v2.0,

Bruker) and Origin (OriginLab).

Peptides and competition binding assays. To assess the influence of peptides on the S1- subunit-ACE2 interaction, binding probabilities were measured before and after tip incubation with 1 µM, 10 µM and 100 µM of peptide. Briefly, a first map was recorded as described above (*i.e.* force volume mode, 1 µm/s approach and retraction speed, ramp size of 500 nm, an applied force of 500 pN, resolution of 32 x 32 pixels and line frequency of 1 Hz, hold time of 250 ms), then the peptide at the appropriate concentration was injected and a new map was recorded.

All the peptides ([22-44], [351-357], [22-57], [22-44-g-351-357]) were synthesized by Genscript (Hong-Kong). Those peptides are designed according to the sequence of the ACE2 receptor in complex with the RBD domain of the S1-glycoprotein.

FD-based AFM and fluorescence microscopy on living cells. AFM (Bioscope Resolve, Bruker) coupled to a confocal microscope (Zeiss LSM-980) were used to acquire correlative images as described.10 The AFM was equipped with a 150 µm piezoelectric scanner. The AFM and the microscope were equipped in a cell-culture chamber allowing maintaining the temperature, the humidity and the CO2 level as described.14 Fluorescence images were recorded using an

oil immersion lens (x100, NA 1.46, Zeiss alpha Plan-Apochromat). PFQNM-LC cantilevers (Bruker) were used to record AFM images (~ 25 µm2) at imaging forces of ~ 500 pN. The cantilevers were oscillated at 0.25kHz with a 750 nm amplitude in the PeakForce Tapping mode. The sample was scanned using 256 pixels per line (256 lines) and a frequency of 0.125 Hz. AFM images and FD curves were analyzed using Nanoscope analysis software, Origin, Gwyddion and ImageJ. Optical images were analyzed using Zen software (Zeiss).

Plasma membrane staining. Plasma membrane-CFP BacMam 2.0 (Invitrogen) was used to check the co-localization of ACE2 protein and plasma membrane according to manufacturer's protocol. Z-stack image was recorded by confocal LSM-980 (Zeiss) using a water immersion lens (x63, NA 1.20, Zeiss C-Apochromat) and 445 nm and 488 nm laser line.

Affinity measurements using biolayer interferometry. Affinity between S1-subunit or RBD and ACE2 was also investigated by biolayer interferometry (BLI), using a Blitz® device equipped with amine reactive 2nd generation (AR2G) biosensors (Pall ForteBio). After hydrating the biosensor for 10 min and performing an initial baseline (10 min), the biosensor surface was chemically activated (5 min) by a freshly prepared 20 mM EDC and 10 mM NHS (in milliQ water) solution. Then, ACE2 (0.025 µg/µL in acetate buffer pH 4) was loaded onto the biosensor during 3 min and the reaction quenched with ethanolamine 1 M (pH 8). After another baseline step (1 min in PBS), binding of S1-subunit or RBD (0.1 mg/mL) was measured for 5 min. Finally, the dissociation step (5 min) was performed in PBS. Data processing and analysis was run using a routine provided by GraphPad Prism.

Declarations

Data availability

The Source data underlying Figs 2c,e-h; 3f,h; 4b-c; 5a are provided as a Source Data file. All other relevant data are available from the corresponding authors upon reasonable request.

Acknowledgments

This work was supported by the Université catholique de Louvain and the Fonds National de la Recherche Scientifique (FRS-FNRS). This project received funding from the European Research Council under the European Union's Horizon 2020 research and innovation program (grant agreement no. 758224) and from the FNRS-Welbio (Grant # CR-2019S-01). The funders had no role in study design, data collection and analysis, decision to publish, or preparation of the manuscript. S. P., A.C.D. and D. A. are Research Fellow, postdoctoral researcher and Research Associate at the FNRS, respectively.

Author contributions

J.Y., S.P., A.C.D. and D.A. conceived the project, planned the experiments, and analyzed the data. J.Y., S.P. and S.D. conducted the AFM experiments. S.P., M.K. and P.S. conducted and analyzed the BLItz experiments. All authors wrote the manuscript.

Competing interests

The authors declare no competing interests.

References

1 Zhou, P. et al. A pneumonia outbreak associated with a new coronavirus of probable bat origin. Nature 579, 270-273, (2020).

2 Tortorici, M. A. & Veesler, D. Structural insights into coronavirus entry. Adv Virus Res 105, 93-116, (2019).

3 Yan, R. et al. Structural basis for the recognition of SARS-CoV-2 by full-length human ACE2. Science 367, 1444, (2020).

4 Gallagher, T. M. & Buchmeier, M. J. Coronavirus spike proteins in viral entry and pathogenesis. Virology 279, 371-374, (2001).

5 Simmons, G., Zmora, P., Gierer, S., Heurich, A. & Pohlmann, S. Proteolytic activation of the SARS-coronavirus spike protein: cutting enzymes at the cutting edge of antiviral research. Antiviral Res 100, 605-614, (2013).

6 Yan, R. et al. Structural basis for the recognition of SARS-CoV-2 by full-length human ACE2. Science (New York, N.Y.) 367, 1444-1448, (2020).

7 Millet, J. K. & Whittaker, G. R. Host cell proteases: Critical determinants of coronavirus tropism and pathogenesis. Virus Research 202, 120-134, (2015).

8 Alsteens, D. et al. Imaging G protein-coupled receptors while quantifying their ligand- binding free-energy landscape. Nature Methods 12, 845-851, (2015).

9 Koehler, M. et al. Glycan-mediated enhancement of reovirus receptor binding. Nature Communications 10, 4460, (2019).

10 Newton, R. et al. Combining confocal and atomic force microscopy to quantify single-virus binding to mammalian cell surfaces. Nature Protocols 12, 2275-2292, (2017).

11 Bell, G. I. Models for the specific adhesion of cells to cells. Science 200, 618-627, (1978).

12 Evans, E., Ritchie, K. & Merkel, R. Sensitive force technique to probe molecular adhesion and structural linkages at biological interfaces. Biophys J 68, 2580-2587, (1995).

13 Evans, E. & Ritchie, K. Dynamic strength of molecular adhesion bonds. Biophysical Journal

72, 1541-1555, (1997).

14 Alsteens, D. et al. Nanomechanical mapping of first binding steps of a virus to animal cells.

Nature Nanotechnology 12, 177-183, (2017).

15 Rankl, C. et al. Multiple receptors involved in human rhinovirus attachment to live cells.

Proceedings of the National Academy of Sciences 105, 17778, (2008).

16 Sieben, C. et al. Influenza virus binds its host cell using multiple dynamic interactions.

Proceedings of the National Academy of Sciences 109, 13626, (2012).

17 Delguste, M. et al. Multivalent binding of herpesvirus to living cells is tightly regulated during infection. Science Advances 4, eaat1273, (2018).

18 Wrapp, D. et al. Cryo-EM structure of the 2019-nCoV spike in the prefusion conformation.

Science 367, 1260, (2020).

19 Shang, J. et al. Structural basis of receptor recognition by SARS-CoV-2. Nature, (2020).

20 Harcourt, J. et al. Isolation and characterization of SARS-CoV-2 from the first US COVID- 19 patient. bioRxiv, 2020.2003.2002.972935, (2020).

21 Jia, H. P. et al. ACE2 receptor expression and severe acute respiratory syndrome coronavirus infection depend on differentiation of human airway epithelia. J Virol 79, 14614-14621, (2005).

22 Zhang, H., Penninger, J. M., Li, Y., Zhong, N. & Slutsky, A. S. Angiotensin-converting enzyme 2 (ACE2) as a SARS-CoV-2 receptor: molecular mechanisms and potential therapeutic target. Intensive Care Med 46, 586-590, (2020).

23 Monteil, V. et al. Inhibition of SARS-CoV-2 Infections in Engineered Human Tissues Using Clinical-Grade Soluble Human ACE2. Cell, (2020).

24 Lan, J. et al. Structure of the SARS-CoV-2 spike receptor-binding domain bound to the ACE2 receptor. Nature, (2020).

25 Wildling, L. et al. Linking of Sensor Molecules with Amino Groups to Amino- Functionalized AFM Tips. Bioconjugate Chemistry 22, 1239-1248, (2011).

26 Butt, H. J. & Jaschke, M. Calculation of thermal noise in atomic force microscopy.

Nanotechnology 6, 1, (1995).

27 Rankl, C. et al. Determination of the kinetic on- and off-rate of single virus-cell interactions. Methods Mol Biol 736, 197-210, (2011).

28 Fiser, A. & Šali, A. in Methods in Enzymology Vol. 374 461-491 (Academic Press, 2003).

Figures

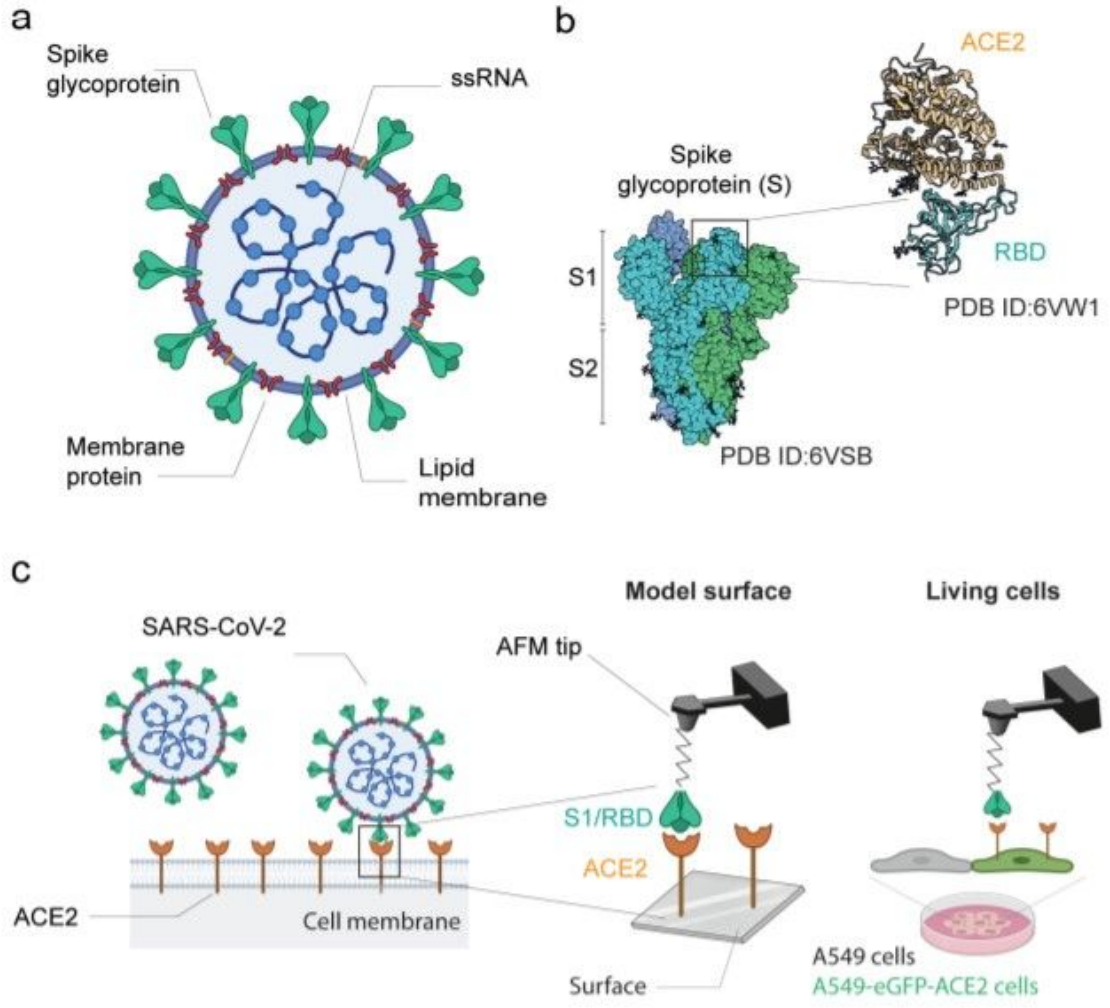

Figure 1

Probing SARS-CoV-2 binding to the ACE2 host receptor. (a) Schematic of SARS-CoV-2 particles, an enveloped ssRNA virus expressing at its surface the spike glycoprotein (S) that mediates the binding to host cells. (b) Structural studies have previously obtained a complex between the receptor binding domain (RBD, a subunit of the S-glycoprotein) and the ACE2 receptor. (c) Schematic of probing SARS-Cov-2 binding using AFM. The initial attachment of SARS-Cov-2 to cells involves specific binding between the viral S-glycoprotein and the cellular receptor, ACE2. The interactions are monitored by AFM on model surfaces, where the ACE2 receptor is attached to a surface and the S1-subunit or the RBD onto the AFM tip, and on A549 living cells expressing or not fluorescently labeled ACE2.

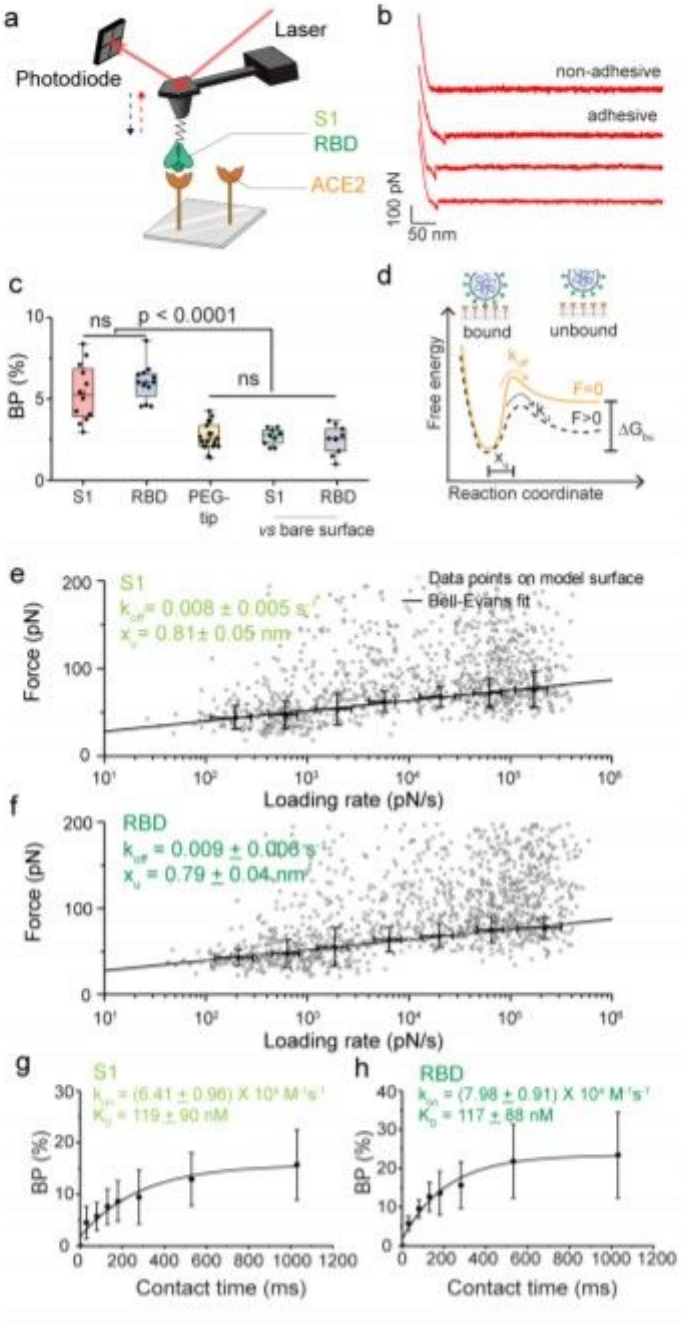

Figure 2

Probing S-glycoprotein binding to the ACE2 host receptor on model surface. (a) Binding of S- glycoprotein subunit (S1 or RBD) is probed on an ACE2-coated surface. (b) Retraction part of four force-distance curves showing either non-adhesive or specific adhesive curves. (c) Box plot of specific binding probabilities (BP) measured by AFM between the functionalized tip (S1, RBD or PEG) and the grafted surface (ACE2 or OH-/COOH- terminated alkanethiol (bare surface). (d) Bell-Evans model describing a virus-receptor bond as a two-state model. The bound state is separated from the unbound state by a single energy barrier located at distance xu. koff and kon represent the dissociation and association rate,

respectively. (e, f) Dynamic force spectroscopy plot (DFS) plot showing the distribution or the rupture forces measured either between the S1-subunit and the ACE2 receptor (N=1052 data points) (e) or between the RBD and the ACE2 receptor (N=1490 data points) (f). The solid line represents the fit of the data with the Bell-Evans fit. (g,h) The BP is plotted as a function of the contact time for S1-subunit and RBD on ACE2 model surfaces and data points were fitted using a least-squares fit of a monoexponential growth. Experiments were reproduced at least 3 times with independent tips and samples. P- values were determined by two-sample t-test in Origin.

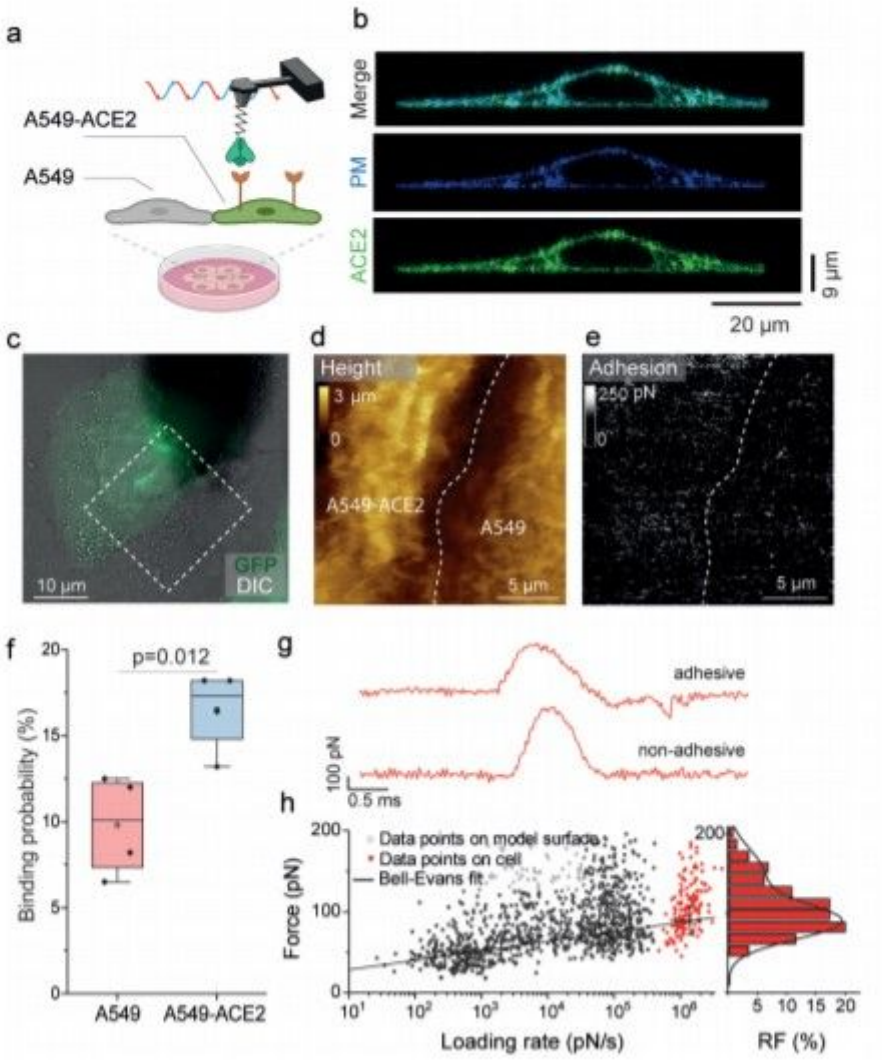

Figure 3

Probing S-glycoprotein binding to the ACE2 host receptor on living cells. (a) Binding of S-glycoprotein subunit-1 (S1) is probed on A549 and A549-ACE2 cells. (b) Confocal microscopy (z-stack) of A549-ACE2-eGFP (green) cell transduced with plasma membrane BFP (blue). (c) Overlay of eGFP and DIC images of a mixed culture of A549 and A549-ACE2-eGFP cells. (d,e) FD-based AFM topography image (d) and corresponding adhesion map (e) in the specified area in c. (f) Box plot of the binding probability between S1 and A549 cells (red) or A549-ACE2 cells (blue). The square in the box indicates mean, the colored box

indicates the 25th and 75th percentile, and the whiskers indicates the highest and the lowest values of the results. The line in the box indicates median. (g) Force vs time curves showing either non-adhesive curve or specific adhesive curve. (h) DFS plot showing the distribution or the rupture forces measured either between the S1 subunit and the ACE2 on model surfaces (black dots, extracted from Figure 2e) and between S1 subunit and ACE2-overexpressing A549 cells (red dots) (N=150). Histogram of force distribution on A549-ACE2 cells is shown on the side. Experiments were reproduced 4 times with independent tips and samples. P-value were determined by two-sample t-test in Origin.

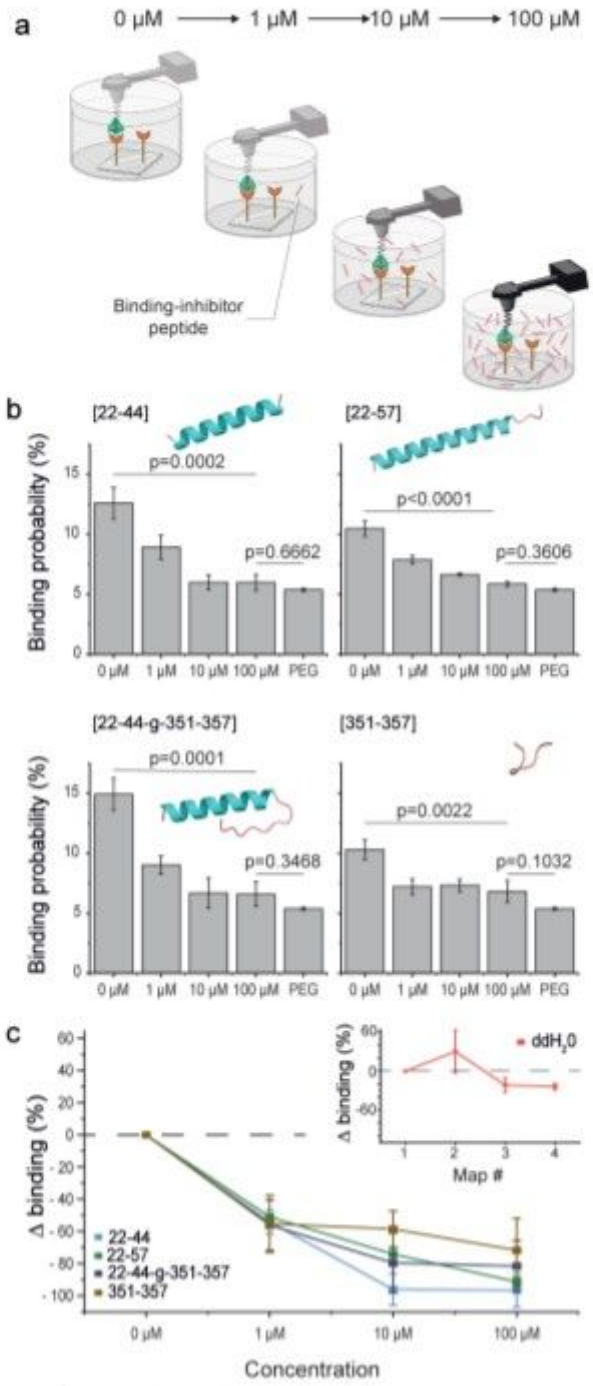

Figure 4

Anti-binding effects of ACE2-derived peptides on S1-subunit binding. (a) Efficiency of blocking peptides is evaluated by measuring the binding probability of the interaction between S1-subunit and ACE2 receptor on model surface before and after incubation of the functionalized AFM tip with the four different peptides at increasing concentration (1-100 µM). (b) Histograms showing the binding probability without peptide 0 µM) and upon incubation with 1, 10 or 100 µM of ACE2-derived peptides ([22-44], [22-57], [22-44-g-351-357] and [351-357]). The binding probability measured with a PEG tip enables to evaluate the non-specific binding level. The prediction of the structure of the ACE-2 derived peptides is shown in insert. The structure of the peptides is based on the structure of the peptide in the crystal structure (PDB ID: 6m0j). For the [22-44-g-351- 357] peptide, its structure was generated using homology modelling.28 (c) Graph showing the reduction of the binding probability. Control with ddH2O is provided in inset showing that repetitive measurements do not result in a similar decrease of the binding probability. Experiments were reproduced at least three times with independent tips and samples. P-value were determined by two-sample t-test in Origin.

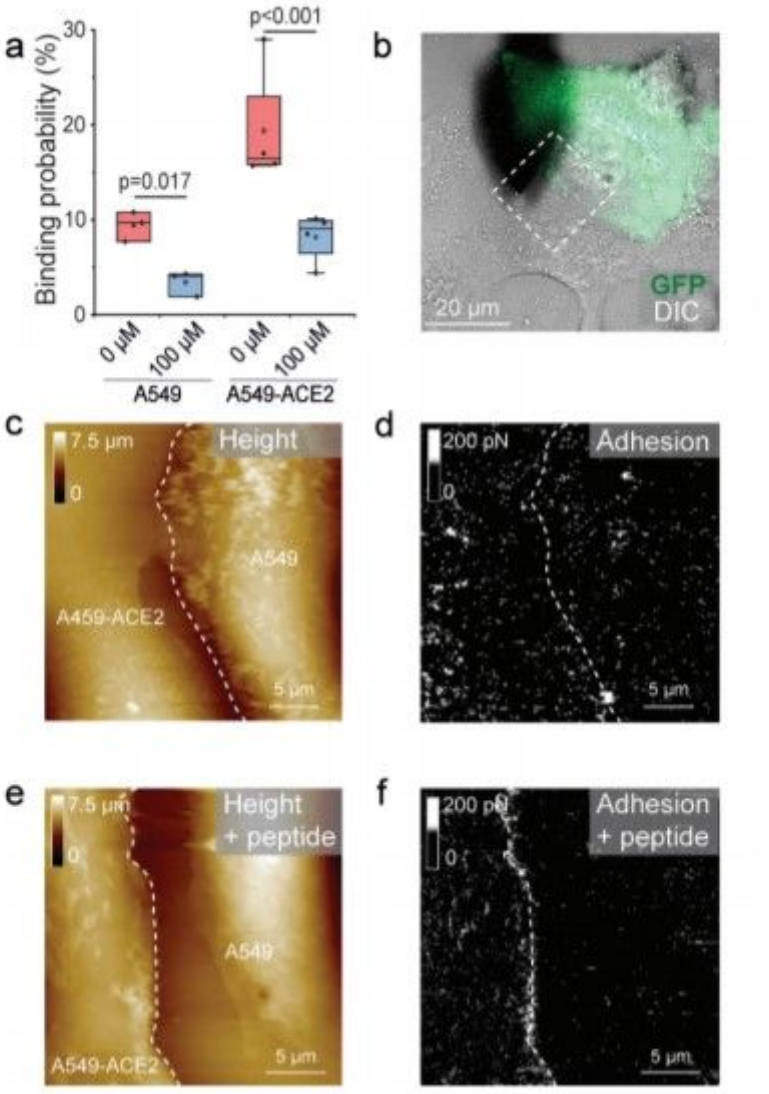

Figure 5

Blocking of S1-subunit binding using ACE2-derived peptide on living cells. (a) Box plot showing the reduction of binding probability measured the S1-subunit derivatized tip and a mixed culture of A549 and A549- ACE2 cells upon injection of the 22-57 ACE2-derived peptide. The square in the box indicates mean, the colored box indicates the 25th and 75th percentile, and the whiskers indicates the highest and the lowest values of the results. (b) Overlay of eGFP and DIC images of a mixed culture of A549 and A549-ACE2-eGFP cells. FD-based AFM topography images (c,e) and corresponding adhesion map (d,f) recorded in the specified area in b (scanned with a scan angle) before (c,d) and after (e,f) incubation of the tip with the 22-57 ACE2-derived peptide. Experiments were reproduced at least three times with independent tips and samples. P-value were determined by two- sample t-test in Origin.

Supplementary Files

This is a list of supplementary files associated with this preprint. Click to download.

- 252160supp322725qzbnz5.pdf